January 1989

Low-Energy Features of the e^--H(n=2) System Exhibited in Fast H^- Detachment Collisions

Chih-Ray Liu
University of Nebraska - Lincoln

Anthony F. Starace
University of Nebraska-Lincoln, astarace1@unl.edu

Low-Energy Features of the e^--H($n=2$) System Exhibited in Fast H^- Detachment Collisions

Chih-Ray Liu and Anthony F. Starace
Department of Physics and Astronomy, The University of Nebraska, Lincoln, Nebraska 68588-0111
(Received 11 August 1988)

Quantitative predictions for the doubly differential detachment collisions, 0.5-MeV $H^- + He \rightarrow H(n=2) + He^* + e^-$, are provided by use of hyperspherical wave functions for the H-e^- system. Individual H-e^- hyperspherical channels are identified as producing distinct "cusp," "shape resonance," and/or "shoulder" features in the laboratory-frame cross sections. Moreover, the first quantitative predictions of the expected Gailitis-Damburg dipole-field–induced oscillations in the cross sections above the H($n=2$) threshold are presented and distinguished from $^1P^\circ$ shape resonance effects.

PACS numbers: 34.50.Fa, 31.20.Di

High-energy negative-ion detachment collisions are important for the production of fast neutral particle beams, which have applications in energy-related technologies. The detachment cross section, particularly that differential in the energy and angle of the detached electron, depends sensitively on the low-energy states of the fundamental H-e^- three-body system. Among the experimental techniques for probing these states are those employing fast H^- beams and the use of kinematic transformations to relate laboratory-frame measurements of detachment cross sections in the forward direction to dynamical behaviors in the H^- projectile frame. Thus, relativistic (i.e., 800 MeV) beams of H^- have been intersected by a laser beam to study the low-energy H^- photodetachment cross section.[1] More recently, nonrelativistic beams of H^- (i.e., 0.1–1.0 MeV) have been used to study the doubly differential detachment cross sections for collisions of H^- on rare-gas targets.[2,3] Of particular interest is the energy region in the vicinity of the H($n=2$) threshold, since electron correlations are essential for excitation plus detachment processes. The observed features[1] in the *photodetachment* cross section near the H($n=2$) threshold have been interpreted theoretically,[4–6] qualitatively most clearly with the hyperspherical coordinate description for the optically allowed (i.e., $^1P^\circ$) final-state channels converging to H($n=2$).[6] We provide here quantitative predictions for the theoretically expected features in doubly differential *collisional detachment* cross sections, using hyperspherical coordinate wave functions for the H-e^- three-body system. In particular, we identify individual projectile-frame hyperspherical channels as producing "cusp," "shape resonance," and/or "shoulder" behaviors in the laboratory-frame cross sections, and we interpret recent measurements[2,3] on the basis of our calculations. Moreover, we provide the first quantitative theoretical predictions of the expected dipole-field–induced oscillations[7] in the cross sections above the H($n=2$) threshold and distinguish these oscillations from $^1P^\circ$ shape resonance effects.

The collision process with which we are concerned is the following:

$$H^- + He \rightarrow H(n=2) + He^* + e^- . \tag{1}$$

Our calculations assume the H^- projectile has the energy 0.5 MeV, employ the closure approximation (in order to sum over all He target final states), treat the scattering process in the first Born approximation, and treat carefully the delicate electron correlations influencing the slow electron detachment from the e^--H($n=2$) system by using the adiabatic approximation[8] to the hyperspherical coordinate Schrödinger equation (with replacement of adiabatic solutions by diabatic ones near the strongly avoided $^1P+$ and $^1P-$ curve crossing[8,9]). This theoretical approach is the same as that described previously[10] for the $H^- + He$ detachment collision in which the H atom is left in its ground state.

In the hyperspherical approach the exact two-electron wave function $\psi(\mathbf{r}_1,\mathbf{r}_2)$ is expanded in a complete set of adiabatic eigenfunctions $\phi_\mu(R,\alpha,\hat{\mathbf{r}}_1,\hat{\mathbf{r}}_2)$, which depend parametrically on a hyperradius $R \equiv (r_1^2 + r_2^2)^{1/2}$ and are functions of the five angular variables $\alpha \equiv \tan^{-1}(r_2/r_1)$, $\hat{\mathbf{r}}_1$, and $\hat{\mathbf{r}}_2$:

$$\psi(R,\alpha,\hat{\mathbf{r}}_1,\hat{\mathbf{r}}_2) \equiv (R^{5/2}\sin\alpha\cos\alpha)^{-1} \sum_\mu F_\mu(R)\phi_\mu(R,\alpha,\hat{\mathbf{r}}_1,\hat{\mathbf{r}}_2) . \tag{2}$$

The ϕ_μ satisfy an angular equation[8–10] having eigenvalue $U_\mu(R)$. The F_μ satisfy a set of coupled radial equations[8–10]; however, in the adiabatic approximation all but the diagonal coupling matrix elements are dropped so that each $F_\mu(R)$ satisfies a one-dimensional radial Schrödinger equation,

$$\left[\frac{d^2}{dR^2} - \left\{ -\frac{U_\mu(R)+1/4}{R^2} - \left\langle \phi_\mu, \frac{d^2\phi_\mu}{dR^2} \right\rangle - \frac{1}{n^2} \right\} + k^2 \right] F_\mu(R) = 0 , \tag{3}$$

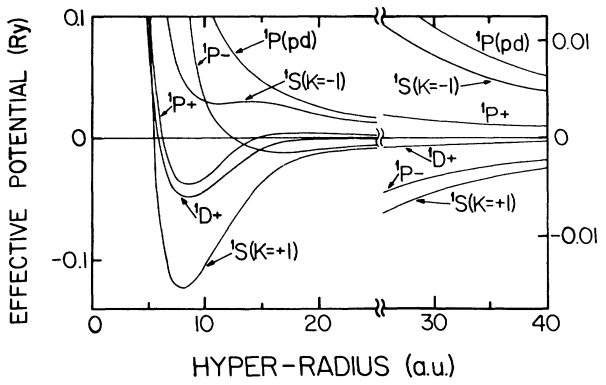

FIG. 1. Effective radial hyperspherical potentials V_μ in Ry plotted vs the hyperradius R for six channels converging to H($n=2$): $^1S(K=\pm1)$, $^1P\pm$, $^1P(pd)$, and $^1D+$. Note that the zero of energy is chosen to be the H($n=2$) threshold and that near $R=25$ the vertical energy scale is changed.

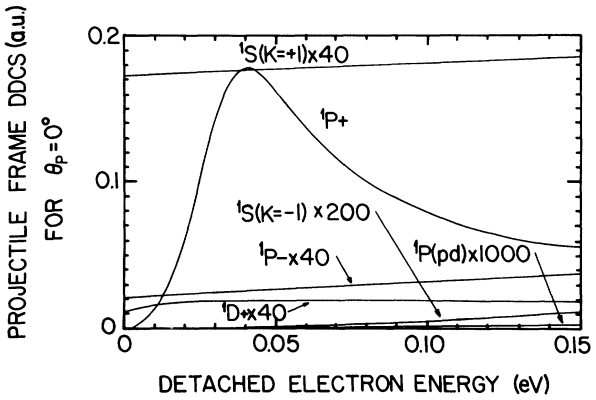

FIG. 2. Projectile-frame DDCS's for process (1) for electrons detached at $\theta_P=0°$ for each of the six hyperspherical channels $^1S(K=\pm1)$, $^1P\pm$, $^1P(pd)$, and $^1D+$ taken separately plotted vs electron energy.

where the effective radial potential $V_\mu(R)$ in curly brackets characterizes the dynamical features of a particular hyperspherical channel μ converging to H($n=2$).

The long-range dipole interaction, due to the degeneracy of the H($n=2$) states,[11] is diagonal in the hyperspherical representation.[6,8] Thus $V_\mu(R)\sim\lambda_\mu(\lambda_\mu+1)/R^2$ as $R\rightarrow\infty$. For λ_μ real, the radial wave function has the asymptotic behavior

$$F_\mu(R)\underset{R\rightarrow\infty}{\sim}(2/\pi k)^{1/2}\sin(kR-\lambda_\mu\pi/2+\delta_\mu)\,, \tag{4}$$

where δ_μ is a phase shift and k is the detached electron's momentum. In this case the threshold behavior of the excitation cross section varies as $k^{2\lambda_\mu+1}$ (i.e., it is zero at threshold). For λ_μ complex, one may write quite generally, $\lambda_\mu=-\frac{1}{2}+i\alpha_\mu$, and one finds,[12]

$$F_\mu(R)\underset{R\rightarrow\infty}{\sim}(2/\pi k)^{1/2}\sin(kR-\pi/4+\theta_\mu+\delta_\mu)\,, \tag{5a}$$

where

$$\theta_\mu\equiv-\tan^{-1}\left\{\frac{\tan[\alpha_\mu\ln(k/2)+x_\mu]}{\tanh[\pi\alpha_\mu/2]}\right\}, \tag{5b}$$

and

$$x_\mu\equiv\arg\Gamma(1-i\alpha_\mu)\,. \tag{5c}$$

In this case, the threshold behavior of the cross section[7] depends on $|k^{\lambda_\mu+1/2}|^2=1$ (i.e., it is finite at threshold). Furthermore, since the experimentally measurable cross sections generally involve contributions from several channels μ, interference terms involving the phases $\theta_\mu+\delta_\mu$ from channels with complex λ_μ introduce oscillations on a scale of $\ln k$.

The effective potentials $V_\mu(R)$ which govern the dynamical features of the doubly differential detachment cross section are shown in Fig. 1 for the six most important channels in the near threshold energy region: $\mu=^1S(K=\pm1)$, $^1P\pm$, $^1P(pd)$, and $^1D+$. The channels μ are identified by total orbital and spin angular momenta as well as by abbreviated labels corresponding to Lin's classification of doubly excited states.[13] We see

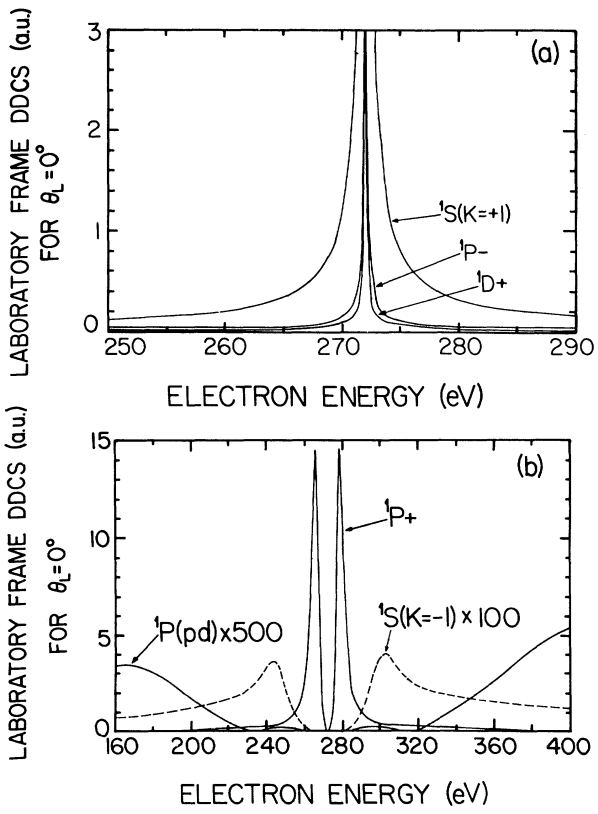

FIG. 3. Laboratory-frame DDCS's for process (1) for electrons detached at $\theta_L=0°$ for each of the six hyperspherical channels taken separately: (a) $^1S(K=+1)$, $^1P-$, and $^1D+$ channels; (b) $^1P+$, $^1S(K=-1)$, and $^1P(pd)$ channels.

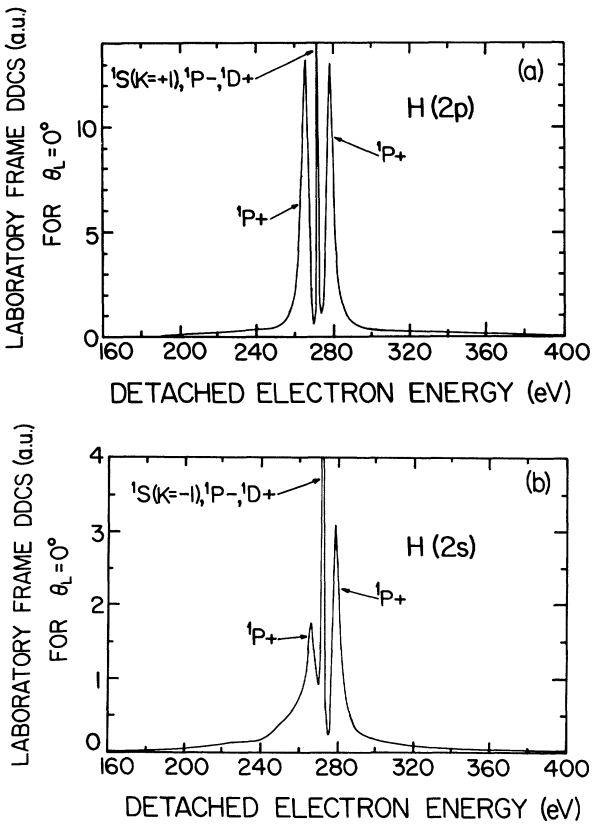

FIG. 4. Laboratory-frame DDCS's for process (1) for electrons detached at $\theta_L=0°$: (a) H(2p); (b) H(2s). The arrows indicate cusp [due to the $^1S(K=+1)$, $^1P-$, and $^1D+$ channels] and shape resonance (due to the $^1P+$ channel) features.

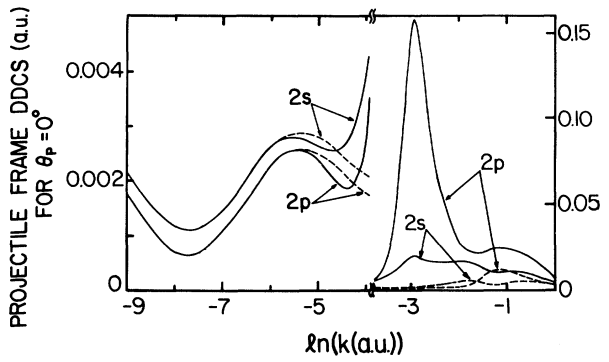

FIG. 5. Projectile-frame DDCS's for process (1) for electrons detached at $\theta_L=0°$ plotted vs ln$k$. Both H(2p) and H(2s) DDCS's are shown. The solid curves include all channels; the dashed ones exclude the $^1P+$ shape resonance channel. Our results assume degeneracy of H(2s) and H(2p) energy levels and therefore may be unreliable for ln$k<-6$. Note the change in vertical scale near ln$k=-4$.

that $^1S(K=-1)$ and $^1P(pd)$ are repulsive potentials, and $^1P+$ has a small barrier at large R which produces shape resonance behavior[4-6]; all have real λ_μ. The $^1S(K=+1)$, $^1P-$, and $^1D+$ potentials are all attractive and have complex λ_μ.

The doubly differential cross sections (DDCS's) for process (1) produced by each of these six channels *taken separately* are given for electrons ejected at zero degress in the projectile frame in Fig. 2 and in the laboratory frame in Fig. 3. One sees that the channels $^1S(K=+1)$, $^1P-$, and $^1D+$ all have finite cross sections at threshold in the projectile (P) frame (Fig. 2), which result in cusp cross sections in the laboratory (L) frame (upon multiplication by the kinematic factor k_L/k_P) at $v_{e^-}=v_{H^-}$ [corresponding to 272 eV in Fig. 3(a)]. The $^1S(K=-1)$, $^1P(pd)$, and $^1P+$ channel cross sections are zero at threshold in the projectile frame (Fig. 2) as well as at $v_{e^-}=v_{H^-}$ in the laboratory [Fig. 3(b)]. On either side of this zero (i.e., at ≈ 266 and ≈ 278 eV) the $^1P+$ channel produces a distinctive shape resonance feature. Analogously, the $^1S(K=-1)$ channel produces broad shoulder features at ≈ 244 and ≈ 303 eV as does the $^1P(pd)$ channel at ≈ 167 and ≈ 407 eV.

When all six hyperspherical channels are added coherently to obtain the partial cross sections for exciting H(2p) or H(2s) simultaneously with electron detachment at $\theta_L=0°$ we obtain the results in Fig. 4. Clearly the dominant features in each cross section are the cusp behavior at ≈ 272 eV, due to the $^1S(K=+1)$, $^1P-$, and $^1D+$ channels, and the $^1P+$ shape resonance features. Interestingly the $^1P+$ feature at ≈ 266 eV in the H(2s) cross section has half the peak height of that at ≈ 278 eV. The shoulder features of the $^1S(K=-1)$ and $^1P(pd)$ channels are not noticeable due to the predominance of the $^1P+$ channel.

Our calculations[14] for 0.5-MeV H^- on He indicate that the DDCS's for H(2p) and H(2s) are very sensitive functions of the electron ejection angle; e.g., the cusp features decrease by 2 orders of magnitude as θ_L increases by a few tenths of a degree.[14] This sensitivity is kinematical, since only near $\theta_L=0°$ does one detect electrons having near zero energy in the projectile frame. The $\theta_L=0°$ results presented here can nevertheless be verified experimentally with current techniques. Thus, Andersen, Bangsgaard, and Sorensen[3(a)] have measured the DDCS for 0.1-MeV H^- on Xe and observe for H($n=2$) both the cusp behavior and two shape resonance features on either side of the cusp. Their projectile energy, however, is rather low for a Born-approximation calculation such as ours. After completing our work, we learned that Duncan and Menendez observe similar features at $\theta_L=0°$ for 0.4-MeV D^- on Ar.[15]

Finally, Fig. 5 shows the first quantitative predictions for the oscillatory behavior that has been predicted[7] for the excitation of the H($n=2$) states near threshold. We plot the projectile-frame DDCS at $\theta_P=0°$ as a function of ln$k$, which is the natural variable [cf. Eq. 5(b)]. This

predicted oscillatory behavior is difficult to observe since for $\ln k > -4$ the $^1P+$ channel introduces shape resonance effects, while for $\ln k < -6$ the detached electron energy becomes comparable with the relativistic and Lamb shift splittings of the degeneracy of the $H(2s)$ and $H(2p)$ states.

We disentangle the shape resonance effect by showing in Fig. 5 results for $H(2p)$ and $H(2s)$ both with and without inclusion of the $^1P+$ channel. Our results for $\ln k < -6$ take no account of the splitting of the $2s$ and $2p$ degeneracy, upon which the predicted[7] dipole-field-induced oscillations depend. Measurement of the predicted features down to $\ln k = -6$, corresponding to 0.1-meV detached electrons, will prove challenging enough.

We gratefully acknowledge extensive discussions with Joseph H. Macek throughout the course of this work. We also thank Chris H. Greene for discussions concerning quantum-defect theory for long-range dipole fields. This work was supported in part by the Department of Energy, Office of Basic Energy Sciences, Division of Chemical Physics.

[1]H. C. Bryant, B. D. Dieterle, J. Donahue, H. Sharifian, H. Tootoonchi, D. M. Wolfe, P. A. M. Gram, and M. A. Yates-Williams, Phys. Rev. Lett. **38**, 228 (1977); see also H. C. Bryant *et al.*, in *Atomic Physics 7,* edited by D. Kleppner and F. M. Pipkin (Plenum, New York, 1981), pp. 29–63.

[2]M. G. Menendez and M. M. Duncan, Phys. Rev. Lett. **40**, 1642 (1978); M. M. Duncan, M. G. Menendez, and J. L. Hopkins, Phys. Rev. A **30**, 655 (1984); M. M. Duncan *et al.*, Phys. Rev. A **34**, 4657 (1986); M. G. Menendez and M. M. Duncan, Phys. Rev. A **36**, 1653 (1987).

[3](a) L. H. Andersen, J. P. Bangsgaard, and J. Sorensen, Phys. Rev. Lett. **57**, 1558 (1986); (b) J. Sorensen, L. H. Andersen, and L. B. Nielsen, J. Phys. B **21**, 847 (1988).

[4]J. Macek, Proc. Phys. Soc. London **92**, 365 (1967).

[5]J. T. Broad and W. P. Reinhardt, Phys. Rev. A **14**, 2159 (1976).

[6]C. D. Lin, Phys. Rev. Lett. **35**, 1150 (1975).

[7]M. Gailitis and R. Damburg, Proc. Phys. Soc. London **82**, 192 (1963), and Zh. Eksp. Teor. Fiz. **44**, 1644 (1963) [Sov. Phys. JETP **17**, 1107 (1963)]; M. Gailitis, in *Atomic Physics 6,* edited by R. Damburg and O. Kukaine (Plenum, New York, 1978), pp. 249–266.

[8]J. Macek, J. Phys. B **1**, 831 (1968).

[9]U. Fano, Rep. Prog. Phys. **46**, 97 (1983).

[10]C. H. Park, A. F. Starace, and J. Macek, Phys. Rev. A **31**, 1336 (1985).

[11]M. J. Seaton, Proc. Phys. Soc. London **77**, 174 (1961).

[12]C. Greene, U. Fano, and G. Strinati, Phys. Rev. A **19**, 1485 (1979). Note that we take θ_μ in the same quadrant as $-\alpha_\mu \ln \frac{1}{2} k - x_\mu$.

[13]C. D. Lin, Phys. Rev. A **29**, 1019 (1984), and Adv. At. Mol. Phys. **22**, 77 (1986). Specifically, our channels μ have the following labels in Lin's $(K,T)^A$ notation: $^1S(K=\pm 1)$: $(\pm 1,0)^+$; $^1P+$: $(0,1)^+$; $^1P-$: $(1,0)^-$; $^1P(pd)$: $(-1,0)^0$; $^1D+$: $(1,0)^+$.

[14]C. R. Liu and A. F. Starace, to be published.

[15]M. M. Duncan and M. G. Menendez, private communication.